Research Square

Preprints are preliminary reports that have not undergone peer review.
They should not be considered conclusive, used to inform clinical practice,
or referenced by the media as validated information.

Observation and identification of autofluorescent urine crystals may be linked to a sign of urolithiasis

Huihua Kenny Chiang (Chiang@nycu.edu.tw)
National Yang Ming Chiao Tung University
Syue-Liang Lin
National Yang Ming Chiao Tung University
Chen-Yuan Chung
National Yang Ming Chiao Tung University
Zih-Ting Chen
National Yang Ming Chiao Tung University
Chih-Chia Huang
National Cheng Kung University
Yun-Zhen Li
National Yang Ming Chiao Tung University
Eric Yi-Hsiu Huang
Taipei Veterans General Hospital

Research Article

Keywords: urine crystal, urolithiasis, autofluorescence, confocal laser scanning microscopy

Posted Date: March 24th, 2022

DOI: https://doi.org/10.21203/rs.3.rs-1476780/v1

License: This work is licensed under a Creative Commons Attribution 4.0 International License.
Read Full License

Abstract

Urolithiasis is a common disease of the urinary system. Its recurrence rate is high and may increase medical expenses. Urine stones are composed of urine crystals and other impurities. We discovered the existence of autofluorescence in some of the urine crystals, especially in urolithiasis patients. The fluorescent molecule existed in urine crystals was verified and identified. We have applied micro-Raman and fluorescence microscopy to classify the urine crystals, used confocal laser scanning microscopy (CLSM) to examine the 3D images and spectra of autofluorescence in crystals, used Fourier transform infrared spectroscopy (FTIR) and mass spectrometry (MS) to identify the type of fluorophore in the autofluorescent urine crystals in urine. Riboflavin was identified as one of the major fluorophores in these autofluorescent urine crystals. The prevalence rates of the autofluorescent crystals in urolithiasis patients and subjects without the history of urolithiasis were to gather statistics. We observed that 80% of urolithiasis patients had autofluorescent crystals. Contrastingly, such crystals existed in only 7% of subjects without the history of urolithiasis. The presence of autofluorescent urine crystals may be linked to a sign of urolithiasis.

Introduction

Urolithiasis is one of the most common urologic diseases; it has a high recurrence rate and results in substantial pain and an increased risk of renal failure.[1–3] The prevalence of urolithiasis is approximately 4–15% in North America, Asia, Europe, and Australia.[4] Urinary stones mainly contain of calcium oxalate dehydrate (COD), calcium oxalate monohydrate (COM), uric acid (UA), hydroxyapatite (HAP), dicalcium phosphate dehydrate (DCPD), struvite, and cystine. After identifying the urine stone type of their patients, clinicians could provide adequate medical treatment and dietary advice to prevent the recurrence of kidney stones.[5]

The formation of urine stones is a multistep process that includes nucleation, growth, aggregation, and retention.[4, 6] The urine stones are composed of urine crystals and other metabolites. The types of crystals in the urine have a high correlation (90.4%) with the composition of urine stones in urolithiasis patients.[7] In a previous study, we found the existence of urine crystals in the urine of over 80% of the urolithiasis patients.[8] Knowing the types of urine crystals maybe helpful in understanding the cause of urolithiasis and further preventing its recurrence.

Manual microscopic examination of urine sediment is the gold standard in clinics for analyzing crystal types based on crystal morphology.[9] Automatic microscopic instruments have been widely used for examining urine sediment in clinical practice, with high-throughput and high concordance rate.[10] All abnormal results identified through the automatic procedure should be further confirmed by manual microscopic examination.[11]

Spectroscopic and imaging techniques have been used for urine crystal analysis. Raman technique has many advantages for analyzing amorphous irregularly shaped urine crystals. Raman spectroscopy is not

affected by water in the surrounding environment, yielding a high signal-to-noise ratio peak, high specificity, and selective qualitative information in biological samples.[12, 13] Micro-Raman spectroscopy (MRS) provide a non-destructive identification of specific vibration peaks in the spectra of urine crystals; the types of the crystals can be characterized accurately and rapidly.[14] Overall, analyzing urine crystals by Raman spectroscopy has the following benefits: (i) simple sample treatment, (ii) independence of water in the environment, (iii) no additional reagents required, and (iv) real-time monitoring.

Chiu et al. developed a nanoplatform, based on Fe_3O_4 nanoparticles, to collect crystals from urine and identify the types of crystals through Raman spectroscopy.[7] Since urine crystals are small, amorphous, irregularly shaped, transparent, and colorless, they are difficult to observe under a microscope. Lo et al. further modified the Fe_3O_4 nanomaterial by labeling dyes (crystal violet) to show the position of crystals for faster automatic crystal analysis.[8] Chen et al. analyzed the urine crystals by micro-Raman system and confocal microscopy for studying the correlation between urine crystals formation and gout patients.[15]

In our recent studies, we discovered that some urine crystals have autofluorescence. To the best of our knowledge, these findings have never been presented in the literature. Furthermore, we found that the autofluorescent urine crystals appeared in most urolithiasis patients. We think it is interesting to identify the type of fluorophores and investigate the role of the existence of the fluorophores in urine crystals. In this study, we aim to characterize the urine crystals through confocal laser scanning microscopy (CLSM) and Fourier-transform infrared spectroscopy (FTIR) and further identify the type of fluorophores present in the autofluorescent urine crystals through mass spectroscopy (MS).

Materials And Methods

Collection, Preparation of Urines, and Crystal Extraction

This study was approved by the Institutional Review Board (IRB) of Taipei Veterans General Hospital (TVGH) and National Yang Ming Chiao Tung University (NYCU). All urine samples from subjects without history of urolithiasis (Group A, n = 15) and patients who had definite diagnosis of urolithiasis (Group B, n = 15) were enrolled. The first morning urine samples were collected for further extraction and characterization. The procedures for the synthesis of Fe_3O_4 nano-platforms and treatment of urine were performed according to the methods reported by Chiu et al..[7] The solution containing Fe_3O_4-bound urine crystals was dropped onto the slide for subsequent crystal analysis. For classifying the crystals, CLSM equipped with the lambda scan equipment for analyzing the autofluorescent images and spectra of the crystals, attenuated total reflectance Fourier transform infrared spectroscopy (ATR-FTIR) for identifying the functional groups of organic fluorophores in the crystals, and mass spectrometry (MS) for determining the molecular weight of fluorophore in crystals.

Micro-Raman Spectroscopy and Fluorescence Imaging

A customized Raman system with a fluorescent microscope was used in this study, and it combined Raman signal measurement, fluorescence imaging, and polarized light imaging to analyze the urine crystals of extracts. For the Raman signal measurement with 50x/100x microscope objectives, the excitation source was a 70 mW 785 nm laser (LASOS, Germany) and a Raman imaging spectrograph (Acton LS785, Princeton Instrument, NJ, USA). The sample was placed on a wet plate to enhance the signal-to-noise ratio. For fluorescence imaging, the mercury lamp and the camera were mounted with an RGB filter set (λ_{ex}: 580 nm bandpass filter (R), 475 nm bandpass filter (G), 434 nm bandpass filter (B);λ_{em}: 630 nm bandpass filter with bandwidth ~ 60 nm (R), 535 nm bandpass filter with bandwidth ~ 38 nm (G), a 470 nm bandpass filter with bandwidth ~ 38 nm (B)). Raman spectra analysis software (WinSpec/32 Ver.2.6.24.0, Roper Scientific and Origin 9, OriginLab Corporation) and image processing software (ImageJ, National Institutes of Health, USA) were used for Raman and fluorescence imaging.

3D Fluorescent Images and Spectral Analysis by CLSM

A confocal laser scanning microscope (CLSM, ZEISS LSM 880 M equipped with Airyscan and QUASAR detectors) was used to acquire and analyze the 3D fluorescence images and spectra of urine crystals. The fluorescence spectra and distribution information of the fluorophores were measured using the 34-channel QUASAR detectors of the CLSM system. For sample preparation, 1 mL of the preprocessed sample was placed on the slide and covered with a cover glass of 0.17 mm thickness, and the slide was mounted. The data were acquired by LSM 880 M and analyzed using image-processing software (ZEN 2.3 SP1 Ver.14.0.0.201, Carl Zeiss). In this experiment, lasers emitting beams of six different wavelengths (405, 440, 458, 488, 514, and 543 nm) were used as excitation sources. The samples were analyzed along the Z-axis to determine the 3D distribution of autofluorescence in the urine crystals.

Functional Groups of Fluorophores Analysis using Micro-ATR-FTIR

A Micro-Attenuated Total Reflection-Fourier Transform Infrared Spectroscopy (micro-ATR-FTIR, Vertex 80v/ Tensor 27, Bruker, Germany, wavenumber range of FTIR: 1100 cm^{-1} to 3750 cm^{-1}) was used to analyze the functional groups in fluorophores non-destructively and conveniently by employing multi-point sampling. The analysis was conducted without further preparation and purification by an 100 µm IR-fiber optic ATR-probe.[16] The ATR technique is a suitable measuring method for analyzing the 10–100 µm urine crystals by using total internal reflection and evanescent wave.

Mass Spectrometry Measurements for Identifying the Fluorophores

Liquid chromatography–tandem mass spectrometry (HPLC/MS-MS, VARIAN 901-MS, Agilent, United States) was used to identify the molecular weights of fluorophores in urine crystals by determining the mass-to-charge ratio (m/z) of the complete structure or fragments of fluorophores. To determine the presence of fluorophores in urine crystals, autofluorescent and non-fluorescent UA and COD urine crystals were used for the mass spectrometry measurements. The ionized components of the samples were

prepared by electrospray ionization (ESI) using a high voltage (4.5 kV) to create an electrospray; this was followed by analysis of these components using mass spectrometry. [17]

Results

Fluorescence Microscopy and Raman Spectroscopy Analysis of Urine Crystals

Image J™ was used to quantify the autofluorescence images of the urine crystals. Figure 1 shows the ambient images of the UA (a), COD (b), and COM (c) urine crystal and the autofluorescence images of crystals excited by a mercury lamp combined with an RGB bandpass filter. The signal-to-background ratios (SBR) of the ROI (region of interest) in autofluorescent urine crystals were 9.85 (UA), 2.81 (COD), and 4.75 (COM).

The crystals were characterized by their corresponding Raman peaks and classified into the appropriate urine crystal categories (UA/ COD/ COM). The Raman spectra of the common urinary crystals were assigned as follows: bands at 999 ± 5 cm^{-1} for UA, 911 ± 5 cm^{-1} and 1,470 ± 5 cm^{-1} for COD, 897 ± 5 cm^{-1}, 1461 ± 5 cm^{-1}, and 1489 ± 5 cm^{-1} for COM. The baselines of spectra were determined by third-order polynomial fitting using the least-squares method, followed by passing the Raman signal through a Savitzky–Golay filter for curve smoothing. The Raman spectra of the clinical urine samples (on the wet slides) are shown in Fig. 2.

We analyzed urine crystals from Group A (subjects without history of urolithiasis) and B (urolithiasis patients). Figure 3a. shows the statistical results of Group A: 66% of the subjects had no crystals, 20% had non-fluorescent COD crystals, 7% had non-fluorescent UA crystals, and only 7% had autofluorescent COM crystals. Figure 3b. shows the statistical results of the Group B: 100% of the subjects had urine crystals, 20% of the patients had non-fluorescent crystals (10% COD, 10% HAP), while 80% of the subjects had autofluorescent crystals (27% UA, 27% COD, 20% COM, 6% HAP). We observed that 12/15 of the urolithiasis patients had autofluorescent crystals in their urine, whereas autofluorescent urine crystals appeared only 1/15 of the subjects without history of urolithiasis; thus the occurrence of autofluorescent crystals was much higher in urolithiasis patients.

Autofluorescence Analysis of the Urine Crystals by CLSM

CLSM was used to analyze the autofluorescence of urine crystals for measuring the 3D fluorescence images along the Z-axis of the crystal by 594 nm excitation. The 2D cross-sectional fluorescent images of the crystals is shown in Fig. 4. The urine crystals collected from the urolithiasis patient emitted strong autofluorescence when excited at 594 nm (He-Ne Laser), which may be due to the presence of fluorophores in the crystals. The emission channel was set to 594–720 nm bandpass filter, and a 100x/NA = 1.4, oil DIC microscope objective was used for 3D confocal imaging. The optical sectioning

thickness was 1.2 μm for analyzing the location of fluorophores. We observed autofluorescence mostly coming from the inside of the crystal.

Figure 5 shows the normalized spectra of the autofluorescent UA, COD, COM urine crystals. The excitation laser wavelength (λ_{ex}) /emission peaks (λ_{em}) were 405/515 ~ 530, 440/520 ~ 565, 458/525 ~ 565, 488/560 ~ 580, 514/580 ~ 590, and 543/590 ~ 635 nm, measured by the CLSM. We also calculated the full width at half maximum (FWHM) of the emission spectra of autofluorescent crystals. The FWHM of emission spectra of autofluorescent UA, COD, and COM were 85–115 nm, 135–195 nm, and 150–200 nm, respectively.

Micro-ATR-FTIR Spectra of Autofluorescent and Non-Fluorescent Urine Crystals

The results of the micro-ATR-FTIR analysis of the three types of urine crystals are shown in Fig. 6; it shows the IR spectra of the autofluorescent urine crystals (UA/COD/COM), standard materials. In the IR absorption spectrum of the UA crystals, we observed the C-N stretching at ~ 1066 cm^{-1}, the C = C stretching peak at ~ 1577 cm^{-1}, the C = O stretching peak at ~ 1641 cm^{-1}, the vibration stretching peaks of the O-H stretching at ~ 2700–3350 cm^{-1}, and the N-H stretching peaks at ~ 2818 and ~ 2988 cm^{-1} in the autofluorescent UA urine crystal.

In the IR absorption spectra of COD and COM crystals, we observed the C-N stretching at ~ 1000 cm^{-1} to 1060 cm^{-1}, the C-O stretching peak at 1317 cm^{-1} to 1323 cm^{-1}, the intense vibration C = O peak at ~ 1614 cm^{-1} to 1615 cm^{-1} (due to the asymmetric COO^- vibration), and the symmetric/asymmetric O-H stretching broad absorption band between 2700 cm^{-1} to 3600 cm^{-1} in the autofluorescent COD/COM urine crystals.[18]

Mass Spectra of Urine Crystals

For further verification of fluorescent objects in the urine crystals, the autofluorescent crystals and non-fluorescent crystals were analyzed by ESI-MS (Fig. 7). Autofluorescent and non-fluorescent crystals were chosen for mass spectrometry and comparison measurement. The data for the UA and COD crystals provided representative results. The signals of m/z were 215.14, 247.17, 279.20, 311.22, 343.25, 375.28, and 445.29 which appeared only in autofluorescent crystals and not in standard materials.

Discussion

Autofluorescence of Urine Crystals

In the statistical results of the autofluorescent crystals (Fig. 3), we observed that urine crystals were more prevalent in urolithiasis patients (100% vs. 34%). The percentage of autofluorescent urine crystals in non-symptomatic patients was 7% which is much lower than the 80% identified within urolithiasis patients. In

those with urine crystals, autofluorescence were more common in urolithiasis patients than in those without history of urolithiasis (80% vs. 20%). Moreover, the highest percentage of urine crystals in both non-symptomatic subjects and urolithiasis patients were COD crystals. Compared to other types of crystals, the autofluorescent UA, COD, and COM urine crystals accounted for 80% of urolithiasis patients. These results match well with the top 3 urine crystals of urolithiasis patients (UA, COD, and COM), which accounted for about 80–90%.[7]

We further analyzed the fluorescent images and spectra of urine crystals using 3D CLSM to determine the fluorophores distribution. The fluorescence images (Fig. 4) showed that the fluorophores were mainly distributed inside the urine crystals. According to the results, it can be understood that the fluorophores were gradually embedded in the interior structure of the urine crystals during their growth process.

The fluorescence spectra of UA/COD/COM urine crystals were further analyzed using an CLSM equipped with the QUASAR system. Figure 5 shows that the autofluorescent urine crystals had different emission peak locations when excited by different lasers. All fluorescent urine crystals (UA/COD/COM) have similar different emission peak locations at 515–530, 520–565, 525–565, 560–580, 580–590, and 590–635 nm upon excitation at 405, 440, 458, 488, 514, and 543 nm, respectively. We speculate that multiple fluorophores contributed to the broadband spectra of fluorescent crystals excited by different lasers.

To clarify whether this broadband result is caused by spectroscopic system factors or multiple fluorophores in urine crystals, we measured the spectrum of the pure fluorophore using CLSM. The results, presented in Fig. S1, show the same peak when it was excited by different lasers. This confirms the patterns of the emission spectra and indicates that the autofluorescent crystals contained multiple fluorophores. We also compared the full width at half maximum (FWHM) of the autofluorescent crystals and pure fluorophore (riboflavin). The FWHM of the emission spectra of riboflavin was maintained at the same value (85 nm, in Fig. S1) and the FWHM of multi-fluorophores were 85–115 nm, 135–195 nm, 150–200 nm for autofluorescent UA, COD, and COM urine crystals in Fig. 5, excited by different lasers. In contrast, the FWHM of autofluorescent crystals containing multiple fluorophores became smaller with excited with longer wavelengths' lasers, while the FWHM of the riboflavin did not change. This phenomenon is attributed to the different extinction coefficient of fluorophores at different laser wavelengths. The spectral overlap percentages of riboflavin and autofluorescent crystals were approximately 73% in UA, 55% in COD, and 48% in COM, indicating that the COM and COD might contain more fluorophores than UA.

Previous studies have shown the existence of flavin-based molecules with emission peaks of fluorescence spectra at ~ 530 nm in urine.[19] We speculated that the emission peaks of fluorescent urine crystals at ~ 510–560 nm might originate from riboflavin fluorophores in the crystals. We found that the autofluorescent urine crystals are mainly composed of different types of fluorophores and UA/COD/COM components.

The Functional Group of Fluorophores in Urine Crystals with Autofluorescence

The difference in FTIR absorption spectra (Fig. 6) between the autofluorescent and non-fluorescent crystals might indicate the IR absorption by the fluorophores in urine crystals. Compared with the non-fluorescent standard materials of UA + COD + COM, the autofluorescent crystals have the following additional or shifted absorption peaks: C-N (~ 1000 to 1060 cm^{-1}), C-O (~ 1324 cm^{-1}), C = O (~ 1655 cm^{-1}), and O-H (2750 to 3750 cm^{-1}), stretching might belong to the functional groups of fluorophores in the crystals. The O-H and C-O stretching only appeared in autofluorescent UA crystals and not in UA standard material. The C = O, C-O, and C-N stretching peaks shifted in autofluorescent COD and COM absorption spectra.

A previous report showed that riboflavin, which has O-H, C = O, C-O, and C-N functional groups in the structure, in urines might promote the formation of urinary stones.[20] This was consistent with the additional peaks and shifted peaks in fluorescent crystals. The IR absorption peaks at 1000 to 1060 cm^{-1} (C-N stretching) and ~ 1654 cm^{-1} (C = O stretching) originated from the structure of the isoalloxazine ring.[21–23] These results were consistent with our inference that riboflavin is most likely the main fluorophore in autofluorescent urine crystals.

The Molecular Weight of Fluorophore in UA/COD/COM Urine Crystals

Figure 7 shows the signals of 215.14, 247.17, 279.20, 311.22, 343.25, 375.28 (m/z) belonged to the fragments of riboflavin by NIST database, which only appeared in the ESI-MS data of the autofluorescent crystals and could be identified. The 375.28 (m/z) was assigned to deprotonated riboflavin (376.37 g/mol, 376.37-375.28 = 1.09 ~ the m/z of H^+, proton). We identified that riboflavin is one of the fluorophores in urine crystals from urolithiasis patients through the FTIR and MS spectra. We did not identify the other fluorophores from the peaks of the MS spectra; this might be caused by the concentrations of other fluorophores in urine crystals were lower than the detection limits, or the m/z of the other fluorophores was out of our measurement range, (m/z > 600).

Implications of autofluorescence urine crystals and urolithiasis

We identified that autofluorescent urine crystals appeared in patients with the definite diagnosis of urolithiasis. The implications were that we discover autofluorescent urine crystals in individuals with ambiguous status of urolithiasis, there are higher chances of diagnosing urolithiasis in such subjects. Our findings may assist in the identifications of urolithiasis in subjects without history of urinary stones. However, a possible artifact is that the urine crystals are soaked in the urine that containing various substrates, so that the autofluorescent molecules in the urine might adsorbed on the surface of urine crystals.

To the best of our knowledge, we presented a novel finding of urine crystals with autofluorescence especially in urolithiasis patients. However, there are some limitations in our study. The samples size of both groups was small. Despite that, the contrasting result of autofluorescent urine crystals in both

groups was so obvious that we are confident that our findings are convincing. We will conduct further studies to enroll more individuals for further analysis. The enrolled subjects without history of urolithiasis may have urinary stones. Such individuals may be patients with early, or insignificant urolithiasis. We seek to answer this specific question in the future study.

Conclusion

In this study, we discovered (1) the existence of autofluorescent urine crystals, and (2) these autofluorescent urine crystals were mostly found in urolithiasis patients. We analyzed the types, images, spectra, functional groups, and fluorophores of urine crystals by using the MRS, CLSM, FTIR, and ESI-MS systems, and identified riboflavin as one of the major fluorophores in the autofluorescent crystals. Autofluorescent urine crystals were found in 80% of the urolithiasis patients, which was much higher than their occurrence in non-symptomatic patients (7%) in the study. The appearance of autofluorescent crystals in urine might be a potential risk indicator and may be linked to an early sign of urolithiasis.

Declarations

Acknowledgments

This research was supported by the Ministry of Science and Technology, Taiwan (NSC 102-2221-E-010-001-MY3, MOST 109-2221-E-010-001-MY3, MOST 109-2218-E-010-002).

Author Contributions Statement

S.L.L. wrote the main manuscript text; C.Y.C., Z.T.C., and Y.Z.L. conducted the experiments and analyzed all of the results in this manuscript. C.C.H. provided some advices about this research. E.Y.H.H. and H.H.K.C. revised the manuscript. All authors reviewed the the manuscript.

Conflict of interest

The authors declare no conflict of interest

References

1. Bihl G, Meyers A. Recurrent renal stone disease—advances in pathogenesis and clinical management. The Lancet. 2001; 358 (9282):651-656.
2. Coe FL, Parks JH, Asplin JR. The pathogenesis and treatment of kidney stones. N Engl J Med. 1992; 327 (16):1141-1152.
3. Worcester EM, Coe FL. Calcium kidney stones. N Engl J Med. 2010; 363 (10):954-963.
4. Basavaraj D, Biyani C, Browning A, Cartledge J. The Role of Urinary Kidney Stone Inhibitors and Promoters in the Pathogenesis of Calcium Containing Renal Stones. EAU-EBU Update Series. 2007; 5:126-136.

5. Han H, Segal AM, Seifter JL, Dwyer JT. Nutritional management of kidney stones (nephrolithiasis). Clin Nutr Res. 2015; 4 (3):137-152.
6. Ratkalkar VN, Kleinman JG. Mechanisms of Stone Formation. Clin Rev Bone Miner Metab. 2011; 9 (3-4):187-197.
7. Chiu Y-C, Chen P-A, Chang P-Y, Hsu C-Y, Tao C-W, Huang C-C, Chiang HK. Enhanced Raman sensitivity and magnetic separation for urolithiasis detection using phosphonic acid-terminated Fe3O4 nanoclusters. J Mater Chem B. 2015; 3 (20):4282-4290.
8. Lo P-A, Huang Y-H, Chiu Y-C, Huang L-C, Bai J-L, Wu S-H, Huang C-C, Chiang HK. Automatic Raman spectroscopic urine crystal identification system using fluorescent image-guided 2D scanning platform with Fe3O4 crystal violet nanoclusters. J Raman Spectrosc. 2019; 50 (1):34-40.
9. Kesson A, Talbott J, Gyory A. Microscopic examination of urine. The Lancet. 1978; 312 (8094):809-812.
10. Fontanella CG, Carniel EL. Computational Tools for the Investigation of the Male Lower Urinary Tract Functionality in Health and Disease. J Med Biol Eng. 2021; 41 (2):203-215. doi:10.1007/s40846-021-00599-y
11. Chien T-I, Kao J-T, Liu H-L, Lin P-C, Hong J-S, Hsieh H-P, Chien M-J. Urine sediment examination: A comparison of automated urinalysis systems and manual microscopy. Clin Chim Acta. 2007; 384 (1):28-34.
12. Krafft C, Steiner G, Beleites C, Salzer R. Disease recognition by infrared and Raman spectroscopy. J biophotonics. 2009; 2 (1-2):13-28.
13. Butler HJ, Ashton L, Bird B, Cinque G, Curtis K, Dorney J, Esmonde-White K, Fullwood NJ, Gardner B, Martin-Hirsch PL. Using Raman spectroscopy to characterize biological materials. Nat Protoc. 2016; 11 (4):664-687.
14. Chiu YC, Yang HY, Lu SH, Chiang HK. Micro-Raman spectroscopy identification of urinary stone composition from ureteroscopic lithotripsy urine powder. J Raman Spectrosc. 2010; 41 (2):136-141.
15. Chen Z-T, Wang C-H, Chiang HK. Characterization of auto-fluorescence urine crystals from gout patients using confocal microscopy and micro-Raman system for urolithiasis prediction. Proceedings of SPIE. 2020; 11359:113591P.
16. Elmer P. FT-IR Spectroscopy Attenuated Total Reflectance (ATR). Technical note. 2005; 27 (11).
17. Ho CS, Lam C, Chan M, Cheung R, Law L, Lit L, Ng K, Suen M, Tai H. Electrospray ionisation mass spectrometry: principles and clinical applications. Clin Biochem Rev. 2003; 24 (1):3.
18. Sekkoum K, Cheriti A, Taleb S, Belboukhari N. FTIR spectroscopic study of human urinary stones from El Bayadh district (Algeria). Arab J Chem. 2016; 9 (3):330-334.
19. Zhang Y, Wang Y, Cao W-W, Ma K-T, Ji W, Han Z-W, Si J-Q, Li L. Spectral characteristics of autofluorescence in renal tissue and methods for reducing fluorescence background in confocal laser scanning microscopy. J Fluoresc. 2018; 28 (2):561-572.

20. Trinchieri A, Lizzano R, Marchesotti F, Zanetti G. Effect of potential renal acid load of foods on urinary citrate excretion in calcium renal stone formers. Urol Res. 2006; 34 (1):1-7.
21. Zheng Y, Dong J, Palfey BA, Carey PR. Using Raman spectroscopy to monitor the solvent-exposed and “buried” forms of flavin in p-hydroxybenzoate hydroxylase. Biochemistry. 1999; 38 (51):16727-16732.
22. Unno M, Sano R, Masuda S, Ono T-a, Yamauchi S. Light-induced structural changes in the active site of the BLUF domain in AppA by Raman spectroscopy. J Phys Chem B. 2005; 109 (25):12620-12626.
23. Pearle MS, Nakada SY. Practical Controversies in medical management of stone disease. vol. 20. Springer; 2014

Figures

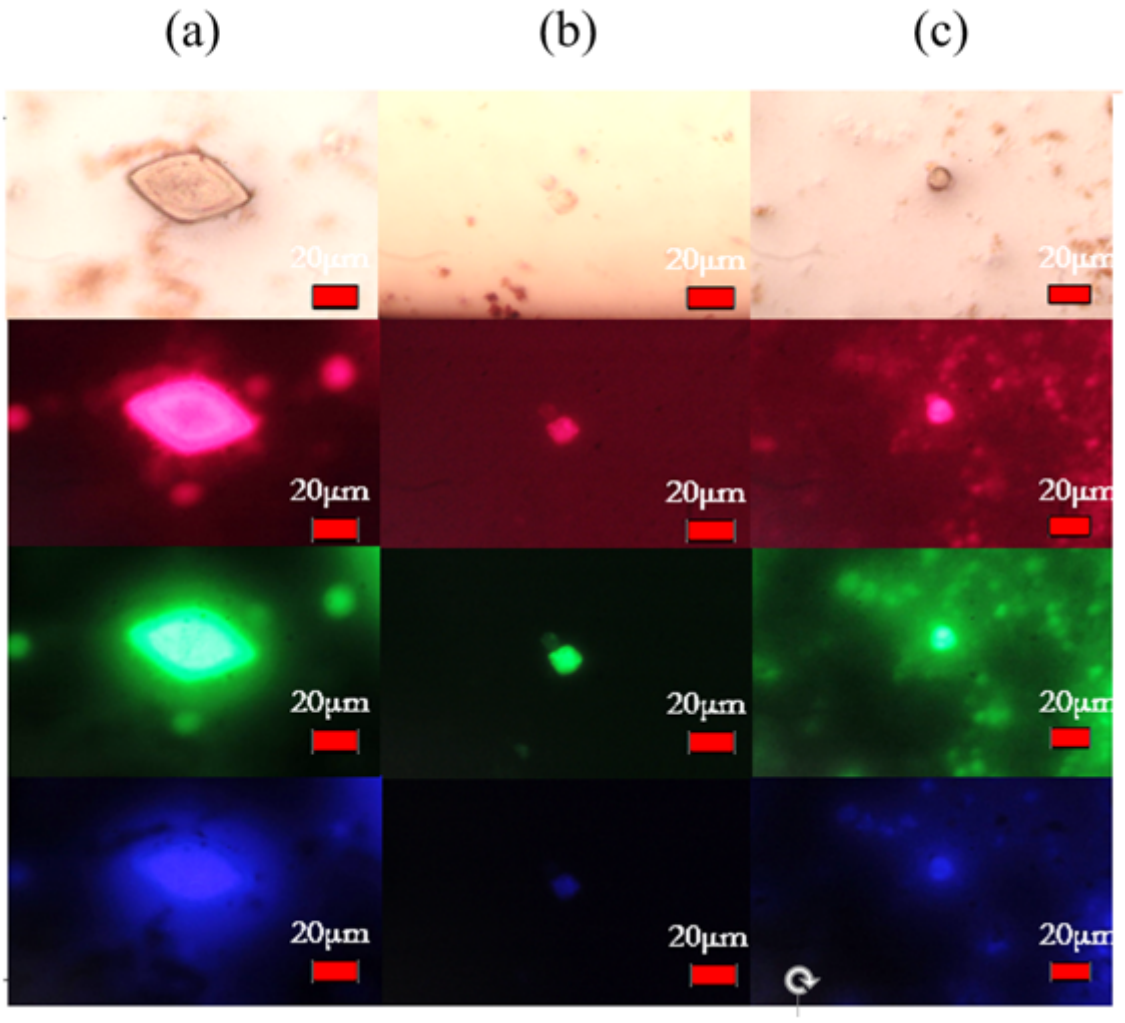

Figure 1

(a) UA, (b) COD, and (c) COM urine crystals under ambient light, and mercury lamp irradiation with the RGB bandpass filter set, respectively.

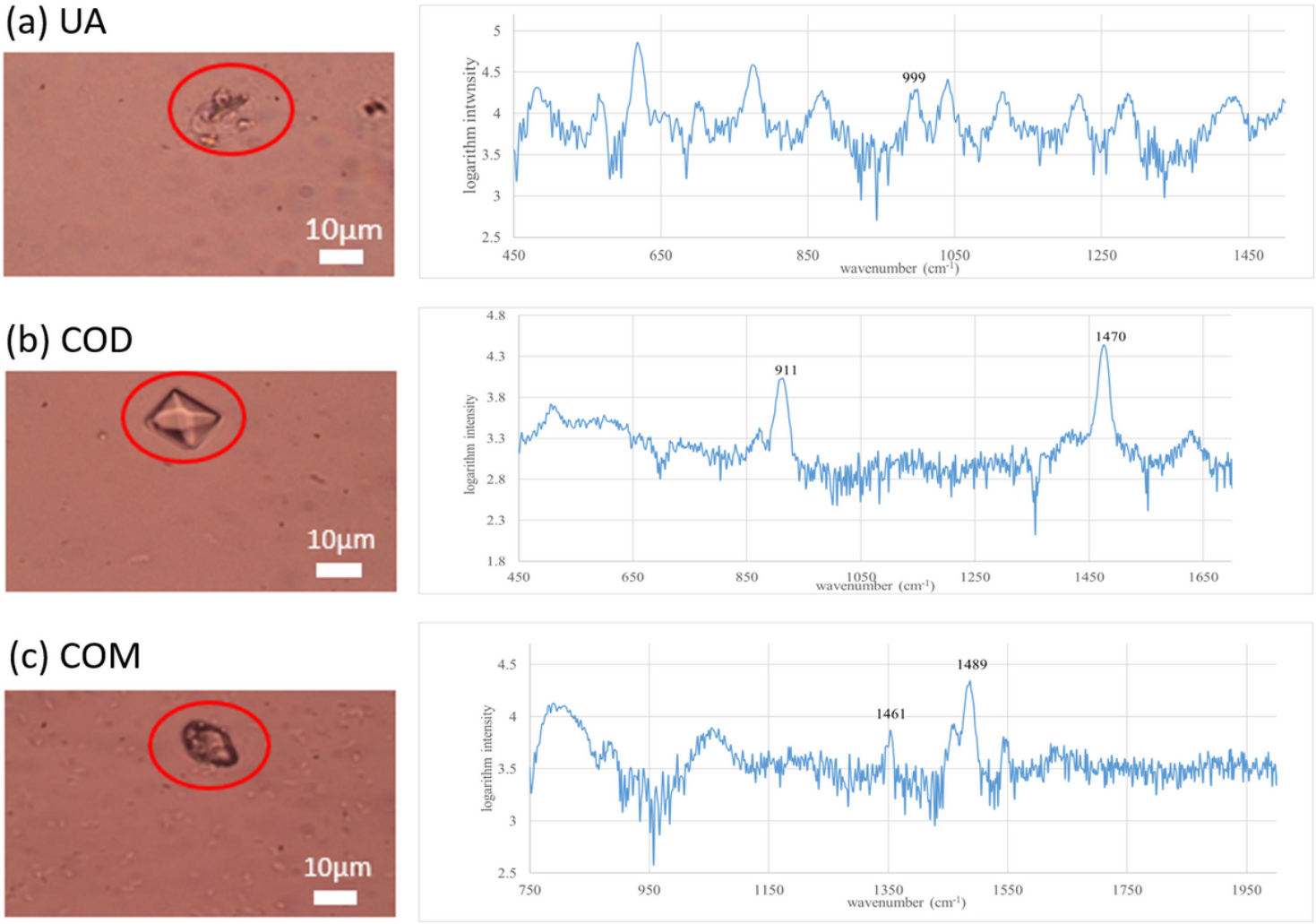

Figure 2

Micro-Raman spectroscopy results of (a) UA, (b) COD, and (c) COM urine crystals.

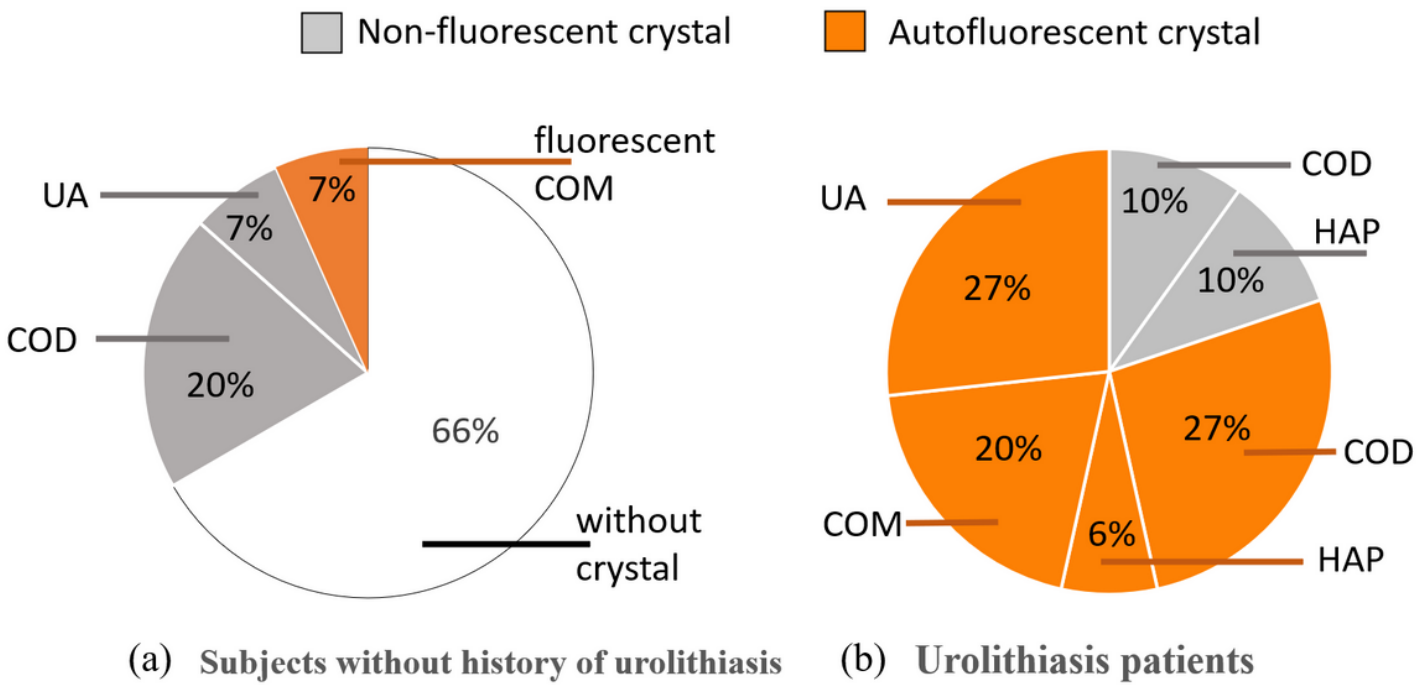

Figure 3

The percentages of autofluorescent crystals that exist in (a) subjects without history of urolithiasis (n=15) and (b) urolithiasis patients (n=15) are 7% and 80%, respectively.

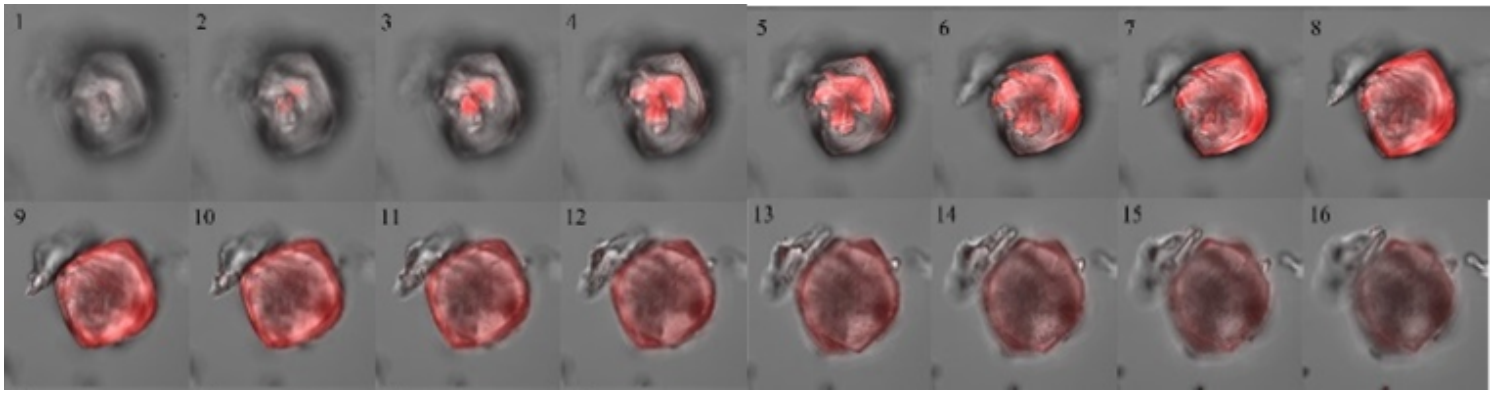

Figure 4

CLSM 3D confocal imaging of a single UA crystal with z-axis scanning with every 1.2 μm step. (λ_{ex}: 594 nm; λ_{em}: 594-720 nm)

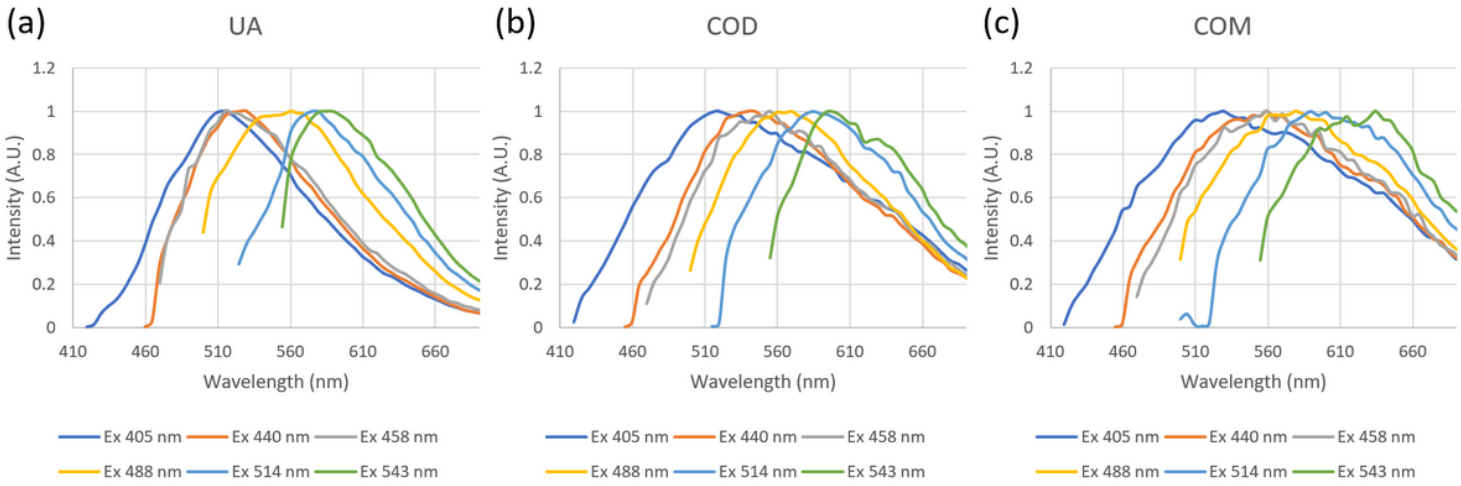

Figure 5

Normalized emission spectra of autofluorescent (a) UA, (b) COD, and (c) COM urine crystal at different excitation wavelengths (λ_{ex}: 405, 440, 458, 488, 514, and 543 nm).

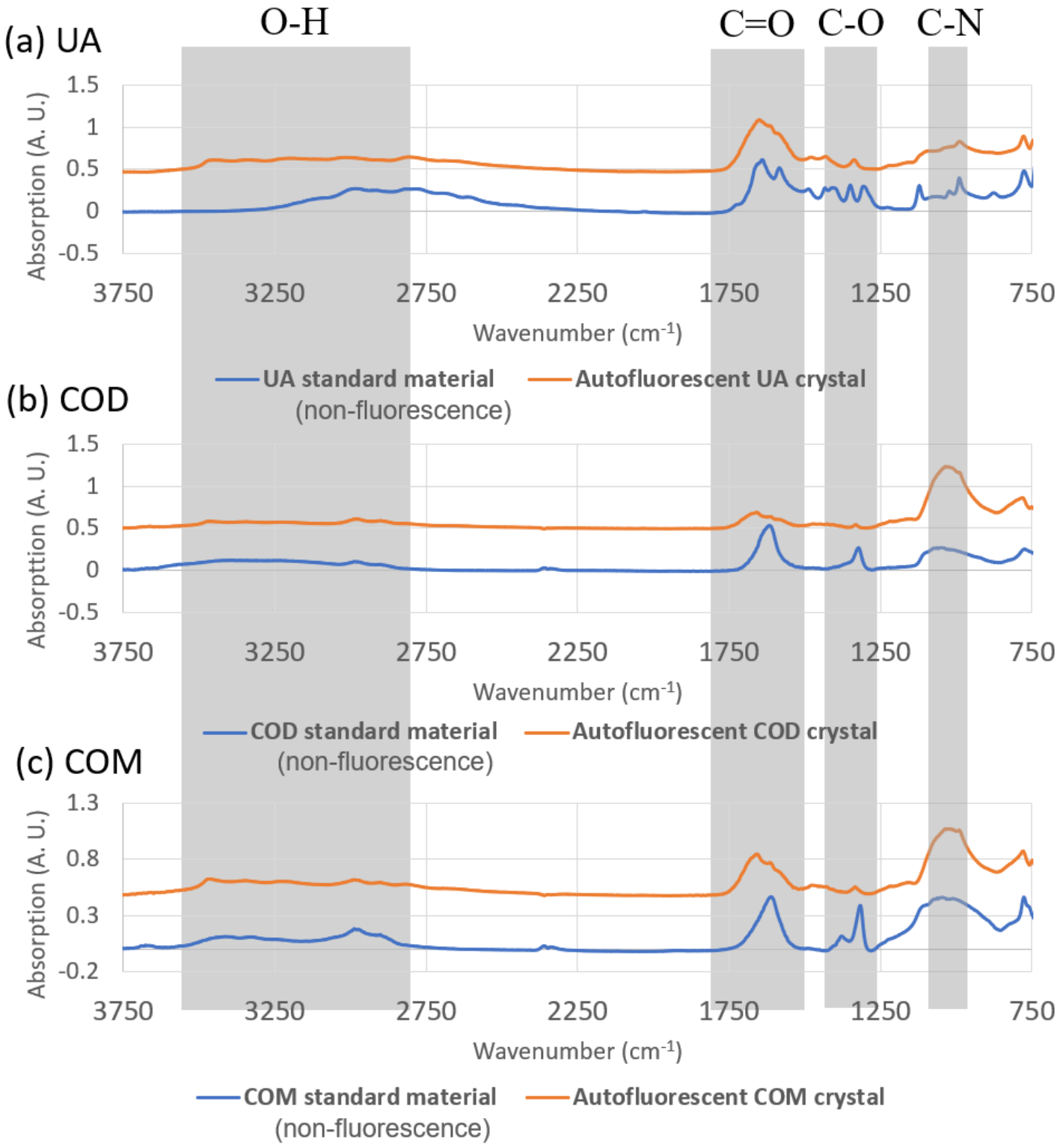

Figure 6

The IR absorption spectra of autofluorescent crystals and standard materials of (a) UA, (b) COD, and (c) COM. The C-N (~1000 cm^{-1} to 1066 cm^{-1}), C-O (1317 cm^{-1} to 1323 cm^{-1}), C=O (~1614 cm^{-1} to 1641 cm^{-1}), and O-H (2700 cm^{-1} to 3600 cm^{-1}) stretching were different between autofluorescent crystals and standard materials.

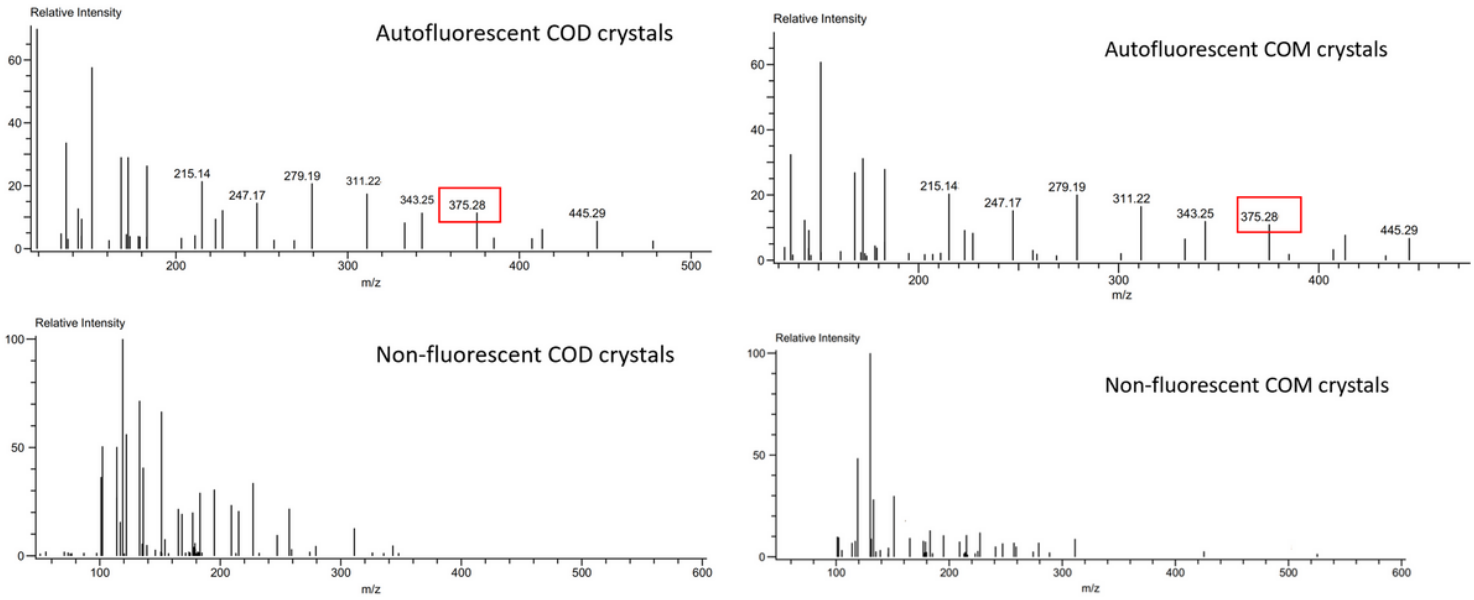

Figure 7

Comparison of MS data of UA and COD urine crystals with and without autofluorescence. The signals of m/z were 215.14, 247.17, 279.20, 311.22, 343.25, 375.28, and 445.29 which only appeared in autofluorescent crystals.

Supplementary Files

This is a list of supplementary files associated with this preprint. Click to download.

- RamancrystalSI.docx